# Nonlinear and Perturbative Evolution of Distorted Black Holes. II. Odd-parity Modes

John Baker[(1)], Steven Brandt[(4)], Manuela Campanelli[(1)], Carlos O. Lousto[(1,5)], Edward Seidel[(1,2,3)] and Ryoji Takahashi[(1)]

[(1)] *Albert-Einstein-Institut, Max-Planck-Institut für Gravitationsphysik, Am Mühlenberg 5, D-14476 Golm, Germany*

[(2)] *National Center for Supercomputing Applications, Beckman Institute, 405 N. Mathews Ave., Urbana, IL 61801*

[(3)] *Departments of Astronomy and Physics, University of Illinois, Urbana, IL 61801*

[(4)] *Department of Astronomy and Astrophysics and Center for Gravitational Physics and Geometry, Pennsylvania State University, University Park, PA 16802*

[(5)] *Instituto de Astronomía y Física del Espacio–CONICET, Buenos Aires, Argentina*

(February 7, 2008)

We compare the fully nonlinear and perturbative evolution of nonrotating black holes with odd-parity distortions utilizing the perturbative results to interpret the nonlinear results. This introduction of the second polarization (odd-parity) mode of the system, and the systematic use of combined techniques brings us closer to the goal of studying more complicated systems like distorted, rotating black holes, such as those formed in the final inspiral stage of two black holes. The nonlinear evolutions are performed with the 3D parallel code for Numerical Relativity, *Cactus*, and an independent axisymmetric code, *Magor*. The linearized calculation is performed in two ways: (a) We treat the system as a metric perturbation on Schwarzschild, using the Regge-Wheeler equation to obtain the waveforms produced. (b) We treat the system as a curvature perturbation of a Kerr black hole (but here restricted to the case of vanishing rotation parameter $a$) and evolve it with the Teukolsky equation The comparisons of the waveforms obtained show an excellent agreement in all cases.

04.25.Dm, 04.30.Db, 97.60.Lf, 95.30.Sf



## I. INTRODUCTION

Coalescing black holes are considered one of the most promising sources of gravitational waves for gravitational wave observatories like the LIGO/VIRGO/GEO/TAMA network under construction (see, e.g., Ref. [1,2] and references therein). Reliable waveform information about the merger of coalescing black holes can be crucial not only to the interpretation of such observations, but also could greatly enhance the detection rate. Therefore, it is crucial to have a detailed theoretical understanding of the coalescence process.

It is generally expected that full scale, 3D numerical relativity will be required to provide such detailed information. However, numerical simulations of black holes have proved very difficult. Even in axisymmetry, where coordinate systems are adapted to the geometry of the black holes, black hole systems are difficult to evolve beyond about $t = 150M$, where $M$ is the mass of the system [3]. In 3D, the huge memory requirements, and instabilities associated presumably with the formulations of the equations themselves, make these problems even more severe. The most advanced 3D calculations based on traditional Cauchy evolution methods published to date, utilizing massively parallel computers, have difficulty evolving Schwarzschild [4], Misner [5], or distorted Schwarzschild [6] beyond about $t = 50M$. Characteristic evolution methods have been used to evolve distorted black holes in 3D indefinitely [7], although it is not clear whether the technique will be able to handle highly distorted or colliding black holes due to potential trouble with caustics.

In spite of such difficulties, much physics has been learned and progress has been made in black hole simulations, in both axisymmetry and in 3D. In axisymmetry, calculations of distorted black holes with [8–10] and without angular momentum [11,12], Misner two black hole initial data, including variations of boosted and unequal mass black holes, have been all been successfully carried out [3,13,14], and the waveforms generated during the collision process have been extensively compared to calculations performed using perturbation theory [15–18]. In 3D, similar calculations have been carried out, especially in evolution of 3D distorted black holes [19] where it was shown that very accurate waveforms can be extracted as a distorted black holes settles down, as is expected to happen when two black holes coalesce.

One of the important results to emerge from these studies is that the full scale numerical and perturbative results agree very well in the appropriate regimes, giving great confidence in both approaches. In particular, the perturbative approach turned out to work extremely well in some regimes where it was not, *a priori*, expected to be accurate. For example, in the head-on collision of two black holes (using Misner data), the perturbative results for both waveforms and energy radiated turned out to be remarkably accurate against full numerical simulations – even in some cases where the black holes had distinct apparent horizons. These impressive agreements have then been improved by the use of second order perturbation theory (see Ref. [17] for a comprehensive review on the Zerilli approach and Ref. [20] for the more recent

curvature based approach holding also for rotating black holes). Study of perturbations also offered the plausible explanation that the peak of the potential barrier that surrounds a black hole was the more relevant quantity, not the horizon. In a more complex application, the collision of boosted black holes was studied. With a small boost, the total energy radiated in the collision was shown to go *down* when compared with the Misner data. Linear theory was able to show that there were two components to the radiation, one from the background Misner geometry and one from the boost. These two components are anti-correlated and combined to produce what has since been called the "Baker dip" [15]. Had there only been a perturbative analysis one might have worried that nonlinear effects might eliminate the dip. Had there been only a full numerical simulation, the dip might have been thought to be evidence of a coding error. When the two were combined, however, a confirmation of the correctness of both procedures was established and the effect understood.

These are just two examples of a rather large body of work that has led to a revival of perturbative calculations, now considered to be used as a tool to aid in the verification and interpretation of numerically generated results. The potential uses of this synergistic approach to black hole hole evolutions, combining both numerical and perturbative evolutions, are many. First, the two approaches go hand-in-hand to verify the full scale nonlinear numerical evolutions, which will become more and more difficult as 3D binary mergers of unequal mass black holes are attempted, with linear, spin, and orbital angular momentum. Second, as the above examples show, they can aid greatly in the interpretation and physical understanding of the numerical results, as also shown in 3D distorted black hole evolutions [19]. Such insight will become more important as we move towards more complex simulations. (As an example of this below, we will show how nonlinear effects and mode-mixing can be understood and cleanly separated from linear effects with this approach.)

Finally, there are at least two important ways in which a perturbative treatment can actually aid the numerical simulation. First, as shown in Ref. [21], it is possible to use perturbative evolutions to provide good outer boundary conditions for a numerical simulation, since away from the strong field region one expects to see low amplitude gravitational waves propagating on a black hole background. This information can be exploited in the outer region in providing boundary data. Second, this combined approach can be used in future applications of perturbative approaches to "take over" and continue a previously computed full scale nonlinear numerical simulation. For example, if gravitational waveforms are of primary interest in a simulation, once the system has evolved towards a perturbative regime (e.g., two coalescing black holes form a distorted Kerr hole, or evolve close enough that a close limit approximation is valid), then one may be able to extract the relevant gravitational wave data, and evolve them on the appropriate black hole background to extract waveforms [22]. Not only would such a procedure save computational time, it may actually be necessary in some cases to extend the simulations. As discussed above, 3D black hole evolutions using traditional ADM style formulations, with singularity avoiding slicings, generally break down before complete wave forms can be extracted. A perturbative approach may be necessary in such cases to extract the relevant waveform physics. This work (called *Lazarus project*) is currently being undertaken by some of the present authors.

However, all work to date in this area of comparing full scale numerical simulations with perturbative approaches has dealt with even-parity distortions of Schwarzschild-like black holes. See for instance Ref. [18], referred to here as Paper I, where we compared perturbative techniques, based on the Zerilli approach, with fully nonlinear evolutions of even-parity distorted black holes. This restriction to the Zerilli equation cannot handle the odd-parity class of perturbations, and more importantly, it cannot be applied easily to the case of rotating black holes. The more general black hole case has both even- and *odd*-parity distortions, and also involves black holes with angular momentum. For this reason, in this paper we take an important step towards application to the more general case of rotating, distorted black holes, by introducing the Teukolsky equation as the fundamental perturbation equation. In fact, for black holes with angular momentum, there is not an $\ell - m$ multipole decomposition of metric perturbations in the time domain and the most natural way to proceed is with the curvature-based perturbation formalism leading to the Teukolsky equation, which also simultaneously handles, in a completely gauge invariant way, both even- and odd-parity perturbations.

The paper is structured as follows. In section II, we review the initial data sets and *four* different techniques and approaches to evolve black holes.

1. We first carry forward the metric-based perturbation approach by considering the Regge-Wheeler (odd-parity) equation to perform perturbative evolutions, and for the first time apply these techniques to a class of distorted black hole data sets containing even-and odd-parity distortions.

2. We also show how one can carry out such perturbative evolutions with the curvature-based Teukolsky equation, using the same initial datasets. Although in certain cases, the metric perturbations can be computed from the curvature perturbations, and vice versa [23], in general using both approaches helps us better to understand the systems we are dealing with.

3. We carry out fully nonlinear evolutions of the same data sets for comparison with a 2D (axisymmetric) code, *Magor*, also capable of evolving distorted rotating black holes.

4. Finally, the same initial data is evolved in its full 3D mode with a general parallel code for numerical relativity, *Cactus*.

In section III we finally discuss the results in detail and show how the combination of these different approaches provides an extremely good and systematic strategy to cross check and further verify the accuracy of the codes used. The comparisons of waveforms obtained in this way show an excellent agreement, in both perturbative and full nonlinear regimes.

Although in this paper we restrict ourselves to the case of initial datasets without angular momentum, the family of datasets we use for this study also includes distorted Kerr black holes, which will be considered in a follow up paper. In fact, our eventual goal is to apply both fully nonlinear numerical and perturbative techniques to evolve a binary black hole system near the merger phase, which final stage can be reasonable modeled by a single distorted Kerr black hole. In this case we should be able to address extremely important questions like how much energy and angular momentum can be radiated in the final merger stage of two black holes.

## II. FOUR WAYS TO EVOLVE DISTORTED BLACK HOLES

### A. Distorted Black Hole Initial Data

Our starting point is represented by a distorted black hole initial data sets developed originally by Brandt and Seidel [8–10] to mimic the coalescence process. These data sets correspond to "arbitrarily" distorted rotating *single* black holes, such as those that will be formed in the coalescence of two black holes. Although this black hole family can include rotation, in this first step we restrict ourselves to the non-rotating limit (the so-called "Odd-Parity Distorted Schwarzschild" of Ref. [8–10]). However, these data sets do include both degrees of gravitational wave freedom, including the "rotation-like" odd-parity modes.

The details of this initial data procedure are covered in [8–10], so we will go over them only briefly here. We follow the standard 3+1 ADM decomposition of the Einstein equations which give us a spatial metric, an extrinsic curvature, a lapse and a shift. We choose our system such that we have a conformally flat three–metric $\gamma_{ij}$ defined by

$$ds^2 = \Psi^4 \left( d\eta^2 + d\theta^2 + \sin^2\theta d\varphi^2 \right). \tag{1}$$

where the coordinates $\theta$ and $\varphi$ are the usual spherical coordinates and the radial coordinate has been replaced by an exponential radial coordinate$\eta$ ($\bar{r} = \frac{M}{2} e^{\eta}$). Thus, if we let the conformal factor be $\Psi = \sqrt{\bar{r}}$ we have the flat space metric with the origin at $\eta = -\infty$. If we let

$$\Psi = \sqrt{\bar{r}} \left( 1 + \frac{M}{2\bar{r}} \right) \tag{2}$$

we have the Schwarzschild 3-metric. In this case one finds that $\eta = 0$ corresponds to the throat of a Schwarzschild wormhole, $\eta = \pm\infty$ corresponds to spatial infinity in each of the two spaces connected by the Einstein-Rosen bridge (wormhole). Note also that this metric is invariant under the isometry operation $\eta \to -\eta$. In the full nonlinear 2D evolution will use this fact to give ourselves the appropriate boundary conditions for making distorted black holes.

The extrinsic curvature is chosen to be

$$K_{ij} = \Psi^{-2} h_{ij} = \Psi^{-2} \begin{pmatrix} 0 & 0 & H_E \\ 0 & 0 & H_F \\ H_E & H_F & 0 \end{pmatrix} \tag{3}$$

where

$$H_E = q_G \left( (n'+1) - (2+n') \sin^2\theta \right) \sin^{n'-1}\theta \tag{4}$$

$$H_F = -\partial_\eta q_G \cos\theta \sin^{n'}\theta \tag{5}$$

$$q_G = Q_0 \left[ \exp\left( -\left(\eta - \eta_0\right)^2 / \sigma^2 \right) + \exp\left( -\left(\eta + \eta_0\right)^2 / \sigma^2 \right) \right]. \tag{6}$$

The various functions have been chosen so that the momentum constraints are automatically satisfied, and have the form of odd-parity distortions in the black hole extrinsic curvature. The function $q_G$ provides an adjustable distortion function, which satisfies the isometry operation, and whose amplitude is controlled by the parameter $Q_0$. This parameter carries units of length squared. Since we will be comparing cases with different masses we will refer to an amplitude $\tilde{Q}_0 = Q_0/M^2$ normalized by the ADM mass of the initial slice. If $Q_0$ vanishes, an unperturbed Schwarzschild black hole results. The parameter $n'$ is used to describe an "odd-parity" distortion. It must be odd, and have a value of at least 3. The function $\Psi$ is the conformal factor, which we have abstracted from the metric and extrinsic curvature according to the factorization given by Lichnerowicz [24]. This decomposition is valuable, because it allows us to solve the momentum and Hamiltonian constraints separately (with this factorization the extrinsic curvature given above analytically solves the momentum constraints).

For the class of data considered here the only nontrivial component of the momentum constraints is the $\varphi$ component:

$$\partial_\eta \hat{H}_E \sin^3\theta + \partial_\theta \left( \hat{H}_F \sin^2\theta \right) = 0. \tag{7}$$

Note that this equation is independent of the function $q_G$. This enables us to choose the solutions to these equations independently of our choice of metric perturbation.

At this stage we solve the Hamiltonian constraint numerically to obtain the appropriate value for $\Psi$. Data at

the inner boundary ($\eta = 0$) is provided by an isometry condition, namely, that the metric should not be changed by an inversion through the throat described by $\eta \to -\eta$. If we allow $Q_0$ to be zero, we recover the Schwarzschild solution for $\Psi$.

The Hamiltonian constraint equation can be expanded in coordinate form to yield, in this case,

$$\frac{\partial^2\Psi}{\partial\eta^2} + \frac{\partial^2\Psi}{\partial\theta^2} + \frac{\partial\Psi}{\partial\theta}\cot\theta - \frac{\Psi}{4} = -\frac{\Psi^{-7}}{4}\left(\hat{H}_E^2\sin^2\theta + \hat{H}_F^2\right). \quad (8)$$

This construction is similar to that given in Bowen and York [25], except that form of the extrinsic curvature is different. The same procedure described above can also be used to construct Kerr and distorted Kerr black holes, as described in Ref. [8–10], but we defer that application to a future paper.

Note that although the form of the extrinsic curvature is decidedly odd-parity (consider reversing the the $\varphi$-direction), the Hamiltonian constraint equation for $\Psi$ affects the diagonal elements of the three-metric producing a nonlinear even-parity distortion. If both $\hat{H}_F$ and $\hat{H}_E$ vanish, undistorted Schwarzschild results. If they are present, they generate a linear odd-parity perturbation directly through the extrinsic curvature, and a second order even-parity perturbation through the conformal factor $\Psi$. Hence, the system will have mixed odd- and even-parity distortions mixed together at different perturbative orders. As we will see below, because even- and odd-parity components are cleanly separated in this way, and the background geometry is explicitly Schwarzschild, it is straightforward to construct analytic, linearized initial data for these distorted black holes, which can then be evolved with the perturbation equations.

In summary, our initial data sets contain both even- and odd-parity distortions of a Schwarzschild black hole, and are characterized by parameters $(Q_0, n', \eta_0, \sigma)$, where $Q_0$ determines the amplitude of the distortion,$n'$ determines the angular pattern, $\eta_0$ determines the radial location (with $\eta_0 = 0$ being the black hole throat), and $\sigma$ determines the radial extent of the distortion. For simplicity of discussion, all cases we will consider in this paper have the form $(Q_0, n', \eta_0 = 2, \sigma = 1)$.

### B. Two Perturbation Formalisms

#### 1. Metric Perturbations

The theory of metric perturbations around a Schwarzschild hole was originally derived by Regge and Wheeler [26] for odd-parity perturbations and by Zerilli [27] for even-parity ones. The spherically symmetric background allows for a multipole decomposition even in the time domain. Moncrief [28] has given a gauge-invariant formulation of the problem, which like the work of Regge-Wheeler and Zerilli, is given in terms of the three-geometry metric perturbations. We will use the Moncrief formalism here as already described in Paper I.

For special combinations of the perturbation equations, a wave equation, the famous Regge-Wheeler equation, resulted for a single function $\phi_{(\ell m)}$:

$$-\frac{\partial^2\phi_{(\ell m)}}{\partial t^2} + \frac{\partial^2\phi_{(\ell m)}}{\partial r*^2} - V_\ell^-(r)\phi_{(\ell m)} = 0\,. \quad (9)$$

Here $r^* \equiv r + 2M\ln(r/2M - 1)$, and the potential

$$V_\ell^-(r) = \left(1 - \frac{2M}{r}\right)\left[\frac{\ell(\ell+1)}{r^2} - \frac{6M}{r^3}\right]. \quad (10)$$

Because we are considering only axisymmetric perturbations all components with $m \neq 0$ vanish identically. We will subsequently suppress the $m$ labels.

Moncrief showed that one can define a gauge-invariant function, that is invariant under infinitesimal coordinate transformations (gauge transformations), which is defined for *any* gauge via

$$\phi_\ell = \frac{1}{r}\left(1 - \frac{2M}{r}\right)\left[c_1^{(\ell)} + \frac{1}{2}\left(\partial_r c_2^{(\ell)} - \frac{2}{r}c_2^{(\ell)}\right)\right] \quad (11)$$

which satisfies the Regge-Wheeler equation above. As the Regge-Wheeler equation is a wave equation, in order to evolve the function $\phi$ we must also provide its first time derivative, which is computed then directly through the definition of the extrinsic curvature of the perturbed Schwarzschild background:

$$\partial_t\phi_\ell = -\frac{2}{r}\left(1 - \frac{2M}{r}\right)\left[\sqrt{1 - \frac{2M}{r}}K^{(\ell)\mathrm{odd}}_{r\varphi} + \partial_r\left(\sqrt{1 - \frac{2M}{r}}K^{(\ell)\mathrm{odd}}_{\theta\varphi}\right) - \frac{2}{r}\sqrt{1 - \frac{2M}{r}}K^{(\ell)\mathrm{odd}}_{\theta\varphi}\right]. \quad (12)$$

This general prescription of linear Schwarzschild perturbations simplifies dramatically in the present case. As discussed in Sec. II A above, the three-metric contains only even-parity perturbations, and those appear *only* at second order. Hence, for linearized treatment both the even- and odd-parity perturbation functions vanish in the initial data! To first order the metric is described by the Schwarzschild background and perturbed initial data consists solely of odd-parity extrinsic curvature contributions. Even-parity modes appear only at higher order, and are not considered in our comparisons here.

For the specific initial data given in the previous section we obtain

$$\phi_\ell\big|_{t=0} = 0 \quad (13)$$

$$\partial_t\phi_\ell\big|_{t=0} = -\frac{2}{r^3}\left(1 - \frac{2M}{r}\right)\left\{-\{r\varphi\}_\ell\, q_G + \{\theta\varphi\}_\ell\left[\partial_\eta^2 q_G + \frac{(7M - 3r)}{r\sqrt{1 - \frac{2M}{r}}}\partial_\eta q_G\right]\right\}, \quad (14)$$

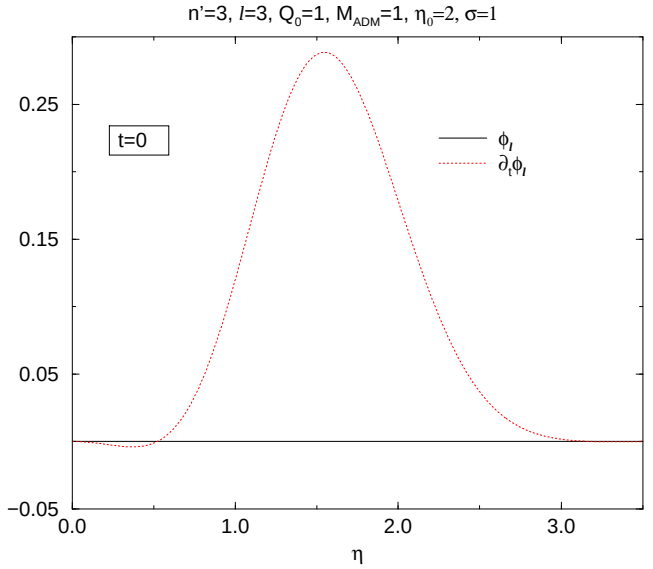


FIG. 1. The initial data for the Moncrief variable. For $n' = 3$ the only linear content is the $\ell = 3$ multipole. The initial value of $\phi$ vanishes for linear odd-parity perturbations, since our choice of initial data only allows for second order even-parity perturbations of the initial three-metric. Our choice of the initial extrinsic curvature generates an almost Gaussian $\partial_t\phi$ that sits near the maximum of the Regge–Wheeler potential.

where for $n' = 3,\ \ell = 3$ and $n' = 5,\ \ell = 3, 5$ the numerical coefficients coming from the multipole decomposition of the extrinsic curvature are

$$\{r\varphi\}_\ell = \frac{2^{(n'-3)/2}(4-\ell)}{(n'-2)(\ell-2)\ell(\ell+2)} \tag{15}$$

$$\{r\theta\}_\ell = \frac{2^{(n'-3)/2}(4-\ell)(\ell+1)}{(n'-2)(\ell-2)\ell}. \tag{16}$$

$$\tag{17}$$

Although these initial data could be obtained numerically via an extraction process described in Paper I [18], it is not necessary to do so in this case with a clear analytic linearization.

In Fig. 1 we plot an example of these analytic initial data. We are now ready to evolve linearly these data with the Regge-Wheeler equation.

### 2. Curvature Perturbations

There is an independent formulation of the perturbation problem derived from the Newman-Penrose formalism [29] that is valid for perturbations of rotating black holes. This formulation fully exploits the null structure of black holes to decouple the perturbation equations into a single wave equation that, in Boyer-Lindquist coordinates $(t, r, \theta, \varphi)$, can be written as:

$$\begin{aligned}
&\left\{ \left[a^2\sin^2\theta - \frac{(r^2+a^2)^2}{\Delta}\right]\partial_{tt} - \frac{4Mar}{\Delta}\partial_{t\varphi} \right.\\
&-2s\left[(r+ia\cos\theta) - \frac{M(r^2-a^2)}{\Delta}\right]\partial_t\\
&+\Delta^{-s}\partial_r\left(\Delta^{s+1}\partial_r\right) + \frac{1}{\sin\theta}\partial_\theta\left(\sin\theta\partial_\theta\right)\\
&+\left(\frac{1}{\sin^2\theta} - \frac{a^2}{\Delta}\right)\partial_{\varphi\varphi} + 2s\left[\frac{a(r-M)}{\Delta} + \frac{i\cos\theta}{\sin^2\theta}\right]\partial_\varphi\\
&\left.-\left(s^2\cot^2\theta - s\right)\right\}\psi = 4\pi\Sigma T\ ,
\end{aligned} \tag{18}$$

where $M$ is the mass of the black hole, $a$ its angular momentum per unit mass, $\Sigma \equiv r^2 + a^2\cos^2\theta$, and $\Delta \equiv r^2 - 2Mr + a^2$. The source term $T$ is built up from the energy-momentum tensor [29]. Gravitational perturbations $s = \pm 2$ are compactly described in terms of contractions of the Weyl tensor with a null tetrad, which components (also given in Ref. [29]) conveniently chosen along the repeated principal null directions of the background spacetime (Kinnersley choice)

$$\psi(t,r,\theta,\varphi) = \begin{cases} \rho^{-4}\psi_4 \equiv -\rho^{-4}C_{n\bar{m}n\bar{m}} & \text{for } s=-2 \\ \psi_0 \equiv -C_{lmlm} & \text{for } s=+2 \end{cases}, \tag{19}$$

where an overbar means complex conjugation and $\rho \equiv 1/(r - ia\cos\theta)$. This field represents either the outgoing radiative part of the perturbed Weyl tensor, $(s = -2)$, or the ingoing radiative part, $(s = +2)$.

For the applications in this paper we will consider $s = -2$, since we will study emitted gravitational radiation and $a = 0$, i.e. perturbations around a Schwarzschild black hole. In general, for the rotating case, it is not possible to make a multipole decomposition of $\psi$ which is preserved in time. So to keep generality we shall use Eqs. (3.1) and (3.2) of Ref. [30] to build up our initial $\psi_4$ and $\partial_t\psi_4$ *not* decompose into $\ell$ multipoles. The analytic expressions for the distorted black hole initial data sets considered in this paper, are:

$$\begin{aligned}
\psi_4\Big|_{t=0} = &-\frac{i}{4}\frac{(1-2\frac{M}{r})}{r^4}\cos\theta\sin^{n'-3}\theta\\
&\Big\{[(n'^2+n'-2)\sin^2\theta - (n'^2-2n'-3)]q_G\\
&+\sin^2\theta[4\sqrt{1-2\frac{M}{r}}\partial_\eta q_G - 2\partial_\eta^2 q_G]\Big\}
\end{aligned} \tag{20}$$

$$\begin{aligned}
\partial_t\psi_4\Big|_{t=0} = &\frac{i}{2}\frac{(1-2\frac{M}{r})}{r^7}\cos\theta\sin^{n'-3}\theta\\
&\Big\{-\sqrt{1-2\frac{M}{r}}r^2\sin^2\theta\partial_\eta^3 q_G\\
&+(5r-12M)r\sin^2\theta\partial_\eta^2 q_G\\
&+r\sqrt{1-2\frac{M}{r}}[(21M-8r+rn'^2+rn')\sin^2\theta
\end{aligned}$$

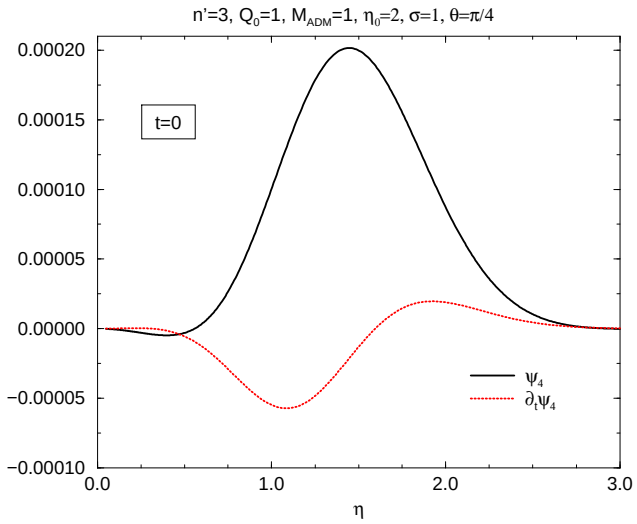


FIG. 2. The initial data for the Weyl scalar $\psi_4$ and its time derivative as given in Eq. (20). The general form of $\psi_4$ resembles that of the Gaussian-like $\partial_t\phi_\ell$. Note that $\partial_t\psi_4$ is nonvanishing in contrast to the initial $\phi_\ell = 0$

$$+(3+2n'-n'^2)r]\partial_\eta q_G + [(n'^2+n'-2)\sin^2\theta$$
$$-(n'^2-2n'-3)](5M-2r)r\ q_G\Big\}. \qquad (21)$$

As expected for pure odd-parity perturbations, only the imaginary part of $\psi_4$ is nonvanishing. Also note that unlike $\phi_\ell = 0$, $\partial_t\psi_4$ does not vanish initially. This is because $\psi_4$ and its time derivative depend on both, the 3-geometry and the extrinsic curvature while the Moncrief function only depends on the perturbed 3-geometry and its time derivative only on the extrinsic curvature. We plot the initial data in Fig. 2. We evolve of these initial data via Teukolsky equation(18) using the numerical method is described in Ref. [31].

Since, after all, we are computing perturbations on a Schwarzschild ($a = 0$) background there must be a way to relate the metric and curvature approaches. In fact the relations between $\psi_4$ and Moncrief even- and odd-parity waveforms in the time domain have been found in Ref. [32] and tested for the even-parity case in Ref. [23]*

Here we can perform the same kind of cross check for the odd parity modes. From the equations in section II.B of Ref. [32] or (2.9) in Ref. [23] we obtain a relation that holds at *all times*

$$\partial_t\psi_4(t,r,\theta,\varphi) = -\frac{i}{8r^2}\sum_\ell \sqrt{\frac{(\ell+2)!}{(\ell-2)!}}\ {}_{-2}Y_\ell(\theta,\varphi)\times$$

$$\Big\{2r\partial_{r^*}\Big[\partial_t\phi_\ell(t,r) - \partial_{r^*}\phi_\ell(t,r)\Big] \qquad (22)$$
$$+2(1-\frac{3M}{r})\Big[\partial_t\phi_\ell(t,r) - \partial_{r^*}\phi_\ell(t,r)\Big] + rV_\ell^-\phi_\ell(t,r)\Big\}$$

and that we can integrate to give us $\psi_4$ from $\phi_\ell$ evolved with the Regge-Wheeler (9) equation instead of evolving $\psi_4$ directly with the Teukolsky equation (18).

### C. Axisymmetric Nonlinear Evolutions

The 2D fully nonlinear evolutions have been performed with a code, *Magor*, designed to evolve axisymmetric, rotating, highly distorted black holes, as described in Ref. [8–10]. *Magor* has also been modified to include matter flows accreting onto black holes [34], but here we consider only the vacuum case.

In a nutshell, this nonlinear code solves the complete set of Einstein equations, in axisymmetry, with maximal slicing, for a rotating black hole. The code is written in a spherical-polar coordinate system, with the rescaled radial coordinate $\eta$ that vanishes on the black hole throat. An isometry operator is used to provide boundary conditions on the throat of the black hole. All three components of a shift vector are employed to keep all off diagonal components of the metric zero, except for the $g_{\theta\varphi}$ component, which carries information about the odd-parity polarization of the radiation. For complete details of the nonlinear code, please see Refs. [8–10,34].

The initial data described in Sec. II A above are provided through a fully nonlinear, numerical solution to the Hamiltonian constraint. The code is able to evolve such data sets for time scales of roughly $t \leq 10^2 M$, and study such physics as horizons and gravitational wave emission.

Consistently with the two different perturbations approaches there are two methods we use to extract information about the gravitational waves emitted during the fully nonlinear simulation: metric based gauge-invariant waveform extraction and direct evaluation of the curvature based Newman-Penrose quantities, such as $\psi_4$.

The first method has been developed and refined over the years [35,36,28,37,38,26] to compute waveforms from the numerically evolved metric. Surface integrals of various metric quantities are combined to build up the perturbatively gauge invariant odd-parity Moncrief functions. These can then be compared directly with the perturbative results.

A second method for wave extraction is provided by the calculation of the Weyl scalar $\psi_4$ which is coordinate invariant but depends on a choice of tetrad basis. For our numerical extractions we follow the method proposed in Ref. [39]. To define the tetrad of their form numerically we thus align the real vector (which can be thought of as providing the spatial components of $l^\mu$ and $l^\mu$) with the radial direction. The complex vectors $m^\mu$ and $\bar{m}^\mu$ point

*Note that this relation among waveforms is only valid at first perturbative order. When nonlinearities are included the two approaches may give widely different results [33].

within the spherical 2-surface. At each step, a Gram-Schmidt procedure is used to ensure that the triad remains ortho-normal. The tetrad assumed by this method is not directly consistent with the one assumed in the perturbative calculation, but for the $a = 0$ it can be made consistent by a type III (boost) null rotation which fixes the relative normalization of the two real-valued vectors. We have found that the transformation $n_P \to A^{-1} l_O$ and $l_P \to A l_O$ where $A = \sqrt{2/(1-2M/r)}$ fixes the normalization appropriately. For the general $a \neq 0$ case this would be insufficient, and we would instead use the more general method proposed in Ref. [30].

### D. Full 3D Evolutions with Cactus

The last of our approaches for evolving these distorted black hole data sets utilizes full 3D nonlinear numerical relativity, and is based on *Cactus*. More general than a numerical code, the *Cactus* Computational Toolkit is actually a general parallel framework for numerical relativity (and other sets of PDE's), that allows users from various simulation communities to gain high performance parallelism on many platforms, access a variety of computational science tools, and to share modules of different evolution methods, initial data, analysis routines, etc. For the relativity community, an extensive suite of numerical relativity modules (or thorns in the language of *Cactus*) is available[†], including black hole and other initial data, slicing routines, horizon finders, radiation indicators, evolution modules, etc.

For this paper, *Cactus* was used to assemble a set of 3D initial data, evolution modules, and analysis routines needed for the comparisons with *Magor* and the two perturbative approaches described above. All operations have been carried out in 3D Cartesian coordinates, from initial data to evolution to waveform extraction. The initial data are computed as in the Magor code, in a polar-spherical type coordinate system, and interpolated onto the Cartesian coordinate system as described in Paper I. The evolutions are carried out with a formulation of Einstein's equations based on the conformal, trace-free approach developed originally by Shibata and Nakamura [40] and Baumgarte and Shapiro [41], and further tested and developed by Alcubierre, et. al., as described in [42,43]. Due to certain symmetries in these initial data sets, the evolutions can be carried out in an octant, in Cartesian coordinates. However, we have chosen in this case to use the full 3D Cartesian grid, as enough memory is now available to run sufficiently large scale evolutions that cover the entire spacetime domain of interest, as would also be necessary when considering the general black hole inspiral problem. For comparison with the 2D code we extract waveforms via the same gauge-invariant Moncrief approach. In this case, surface integrals are carried out on the Cartesian based system by coordinate transformations and interpolation onto a coordinate 2–sphere, as described in Ref. [19].

Further details of the individual simulation parameters are provided as needed when discussing the results below.

[†] *Cactus* is well documented and can be downloaded freely from a web server at http://www.cactuscode.org. For more information on *Cactus*, its use in numerical relativity and other fields, please see the web pages.

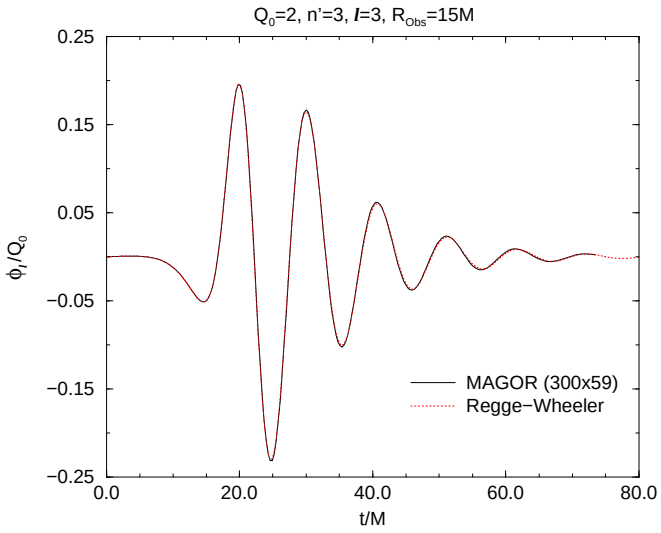


FIG. 3. The $\ell = 3$, odd-parity Moncrief waveform, extracted from the fully nonlinear 2D evolution code (solid line) and compared to the fully linear evolution of the same data, obtained by the Regge-Wheeler equation, for the low amplitude case ($Q_0 = 2, n' = 3, \eta_0 = 2, \sigma = 1$). The excellent agreement shows that both approaches are accurate, and that the black hole physics is operating in the linear regime.

## III. RESULTS

Here we compare the results of evolving the odd-parity distorted black holes by the four techniques described above. We consider two classes of distortions ($n' = 3$ and $n' = 5$) with different angular distributions, and various amplitudes to include cases of linear and distinctly nonlinear dynamics. For the $n' = 3$ case the distortion is (linearly) pure $\ell = 3$, while the $n' = 5$ case encodes a mix of $\ell = 3$ and $\ell = 5$ distortions in the initial data.

### A. Comparison of Nonlinear Evolutions with Regge-Wheeler Theory

In this subsection we compare the 2D nonlinear (*Magor*) evolutions with the results of the Regge-Wheeler perturbative approach. We first consider the nonlinear evolution of a family of data sets with parameters $(Q_0, n' = 3, \eta_0 = 2, \sigma = 1)$.

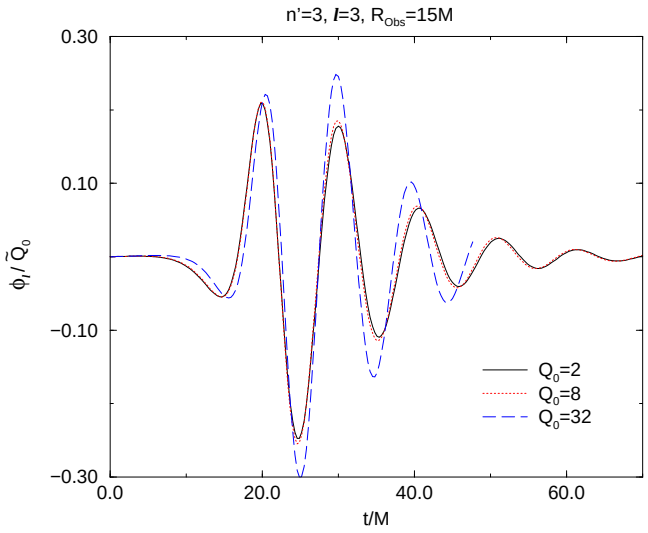


FIG. 4. The $\ell = 3$, odd-parity Moncrief waveform, extracted from the fully nonlinear 2D evolution code, for a series of evolutions with initial data parameters $(Q_0, n' = 3, \eta_0 = 2, \sigma = 1)$. The waveforms are extracted at isotropic coordinates $\bar{r} = 15M$. For $n' = 3$ we only have $\ell = 3$ linear contributions. We normalized waveforms by the amplitude $\tilde{Q}_0$ in order to study the linear and nonlinear regimes. It is observed that for $Q_0 \leq 8$ the linear regime is maintained, while for $Q_0 = 32$ nonlinearities are well noticeable. The effect of nonlinear contributions increases the scaled amplitude of the waveform and increases its frequency. This indicates that the final ringing black hole is significantly smaller than the initial mass of the system.

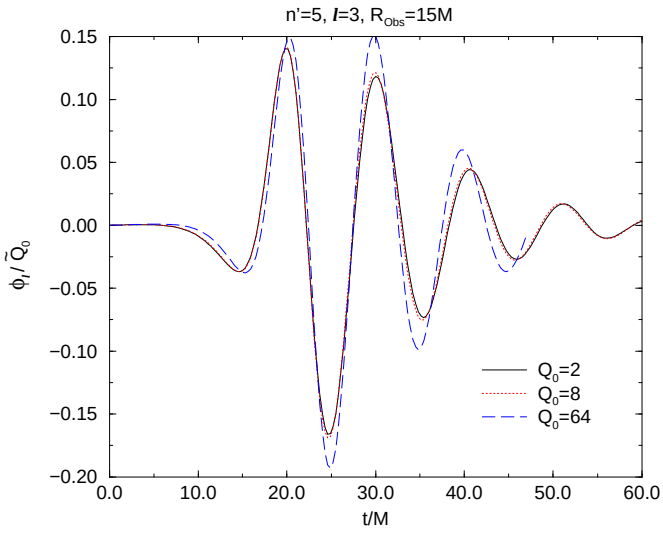


FIG. 5. We show the $\ell = 3$ normalized odd-parity Moncrief waveform for $(Q_0, n' = 5, \eta_0 = 2, \sigma = 1)$ initial data, extracted from the fully nonlinear 2D code for a variety of amplitudes $Q_0$. Again, the system is clearly linear for $Q_0 \leq 8$ and nonlinearities cause an increase in amplitude and frequency of the wave.

For low amplitude cases with $Q_0 < 8$, we are in the linear regime and even the nonlinear evolutions exhibit strongly linear dynamics. In Fig. 3 we show $\ell = 3$ waveform results obtained from the 2D nonlinear code, for the case $Q_0 = 2$, and compare with Regge-Wheeler evolutions of the $(\phi, \partial_t \phi)$ system. The agreement is so close that the curves cannot be distinguished in the plot. The perturbative-numerical agreement is equally good with the other linear waveforms at low amplitude so we will leave the perturbative results out of the plots and focus on the transition to nonlinear dynamics.

In Fig. 4 we show the $\ell = 3$ gauge-invariant Moncrief waveforms for a sequence of such evolutions of increasing amplitude $Q_0$. The waveforms have all been normalized by the amplitude factor $\tilde{Q}_0 = Q_0/M^2$ to accentuate nonlinear effects. If the system is in the linear regime, the normalized waveforms will all line up, as is clearly the case in the regime $Q_0 \leq 8$. For the large amplitude case $Q_0 = 32$, the normalized waveform is much larger, indicating that here we are well into the nonlinear regime.

We now consider the transition to nonlinear dynamics in our second family of data sets, given by parameters $(Q_0, n' = 5, \eta_0 = 2, \sigma = 1)$. These data sets have a linear admixture of both $\ell = 3$ and $\ell = 5$ perturbations, and should contain waveforms of both types. In Fig. 5, we show the results of the fully nonlinear evolution with the *Magor* code in maximal slicing, extracting the $\ell = 3$ gauge-invariant Moncrief waveform for various amplitudes. The waveforms are again normalized by the amplitude factor $\tilde{Q}_0$. In this case the nonlinearity is somewhat weaker at $Q_0 = 32$ so we have included the $Q_0 = 64$ curve in the figure. For the $\ell = 5$ case, shown in Fig. 6, the higher frequency of the quasi-normal ringing makes it easier to appreciate the nonlinearities at $Q_0 = 32$. The plots indicate that again the dynamics are quite linear below $Q_0 = 8$

The waveforms we have shown so far are the only ones predicted to linear order in perturbation theory. We would need to apply higher order perturbation theory to predict waveforms for the even-parity or higher-$\ell$ odd parity modes. Nevertheless general considerations from the perturbative point of view do provide some expectations on the scaling of the other nonlinear waveform modes within the families considered here. We return to the $n' = 3$ family for an example. The leading contribution to the $n' = 3$, $\ell = 5$ odd-parity waveform comes from the cubic coupling of the first order $\ell = 3$ odd-parity mode discussed above (including the coupling of the $\ell = 3$ odd-parity mode with the second order even-parity $\ell = 2$ mode expected via the source term contribution to the solution of the Hamiltonian constraint in the initial data. Thus, this wave component should appear at the third perturbative order. We verify this expectation by plotting the numerical results for the $\ell = 5$ odd-parity waveforms scaled this time by $\tilde{Q}_0^3$ in Fig 7. Although the magnitudes of these waveforms are far smaller than those of the $\ell = 3$ mode we again see very nice agreement, below $Q_0 = 8$, with the perturbative expectation, that the waveforms should superpose.

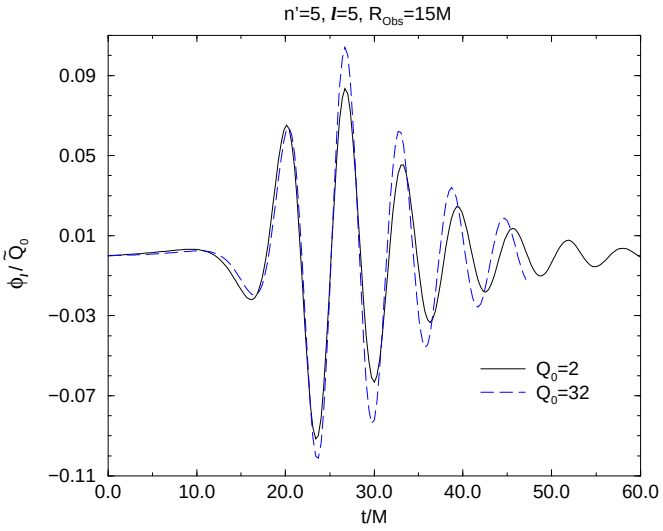


FIG. 6. We show the $\ell = 5$ normalized odd-parity Moncrief waveform for $(Q_0, n' = 5, \eta_0 = 2, \sigma = 1)$ initial data, extracted from the fully nonlinear 2D code for a variety of amplitudes $Q_0$. The regime is clearly linear for $Q_0 = 2$ and nonlinear components appear for $Q_0 = 32$. The increase in frequency and amplitude of the wave are seen here also.

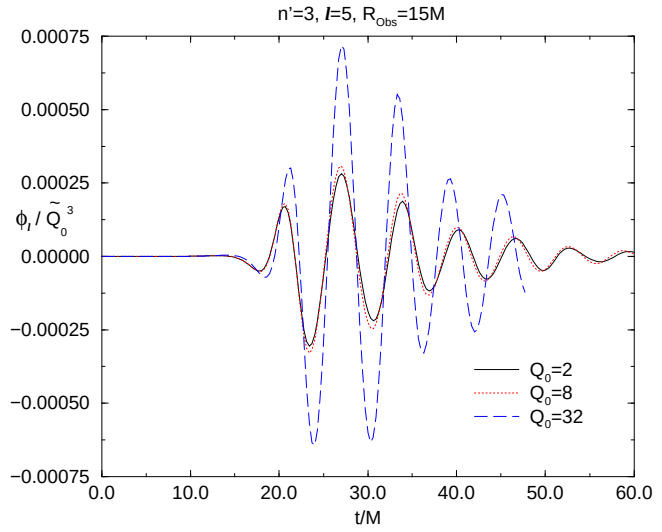


FIG. 7. The Moncrief waveform for a purely nonlinear mode. For $n' = 3$, the $\ell = 5$ multipole is generated by cubic products of the odd-parity wave (squares generate even-parity ones). Accordingly we normalized waveforms by $Q_0^3$. Still higher nonlinearities switch on for $Q_0 = 32$ and show the generic increase in the frequency of the wave.

Let us now take another look at Figs. 4-6 to consider what is happening as we move into the nonlinear regime where the waveforms no longer superpose. In all the graphs we see the same general features arising as begin to drive the system into the nonlinear regime. These are higher frequency ringing, and larger amplitudes for the later parts of the waveform. At $Q_0 = 32$ the $n' = 3$ case shows a roughly 10% increase in frequency compared to 5% for the $n' = 5$ case. Since the final state of the system will be a black hole, we expect quasi-normal ringing in the late-time behavior of the system regardless of the size of the initial perturbations. This is indeed what we see in the waveforms, except that the ringing is at a higher frequency (relative to the initial mass of the system) than we expected. This indicates that the mass of the final ringing black hole has less mass than the ADM mass of the initial data. The perturbations have grown large enough to generate radiation amounting to a noticeable fraction of the total ADM mass leaving behind a slightly smaller black hole. The smaller mass of the final black hole is also consistent with a larger amplitudes, since the scaled perturbation $\tilde{Q}_0 = Q_0/M^2$ is larger relative to a smaller mass black hole. The arrival time of the wave pulse is not strongly affected by the change in mass because the time and wave extraction points are both scaled against the initial mass.

### B. Comparison of Nonlinear Evolutions with Teukolsky Theory

We now turn to the curvature based Teukolsky approach to perturbative evolution for black hole spacetimes. As motivated above, this is a much more powerful approach that will enable perturbative evolutions of both polarizations of the gravitational wave, and evolutions of distorted black holes with angular momentum, and without the need for multipolar expansions. The key difference for analysis within this (Teukolsky) formalism is that , in the general case, we no longer have the benefit of a time-independent separation into multipoles. In this first step towards the transition between the metric perturbation (Moncrief) approach and the curvature based (Teukolsky) approach, we consider the same data sets studied above, which have linear perturbations only for odd-parity, nonrotating black holes. We will consider more general systems in future papers.

We now consider evolutions of the distorted black hole data set $(Q_0 = 1, n' = 3, \eta_0 = 2, \sigma = 1)$. The perturbative initial data for $\psi_4$ and $\partial_t \psi_4$, needed for use in the Teukolsky evolution, have been obtained as described in Sec. II B 2 above. These data are then evolved and recorded at the same coordinate location as before $(r = 15M)$ for comparison with the previous results. In Fig. 8 we show the results of the full 2D nonlinear evolution, obtained with *Magor* in maximal slicing, the Teukolsky evolution, and the Regge-Wheeler evolution obtained previously. The solid line shows the results of $\psi_4$ obtained

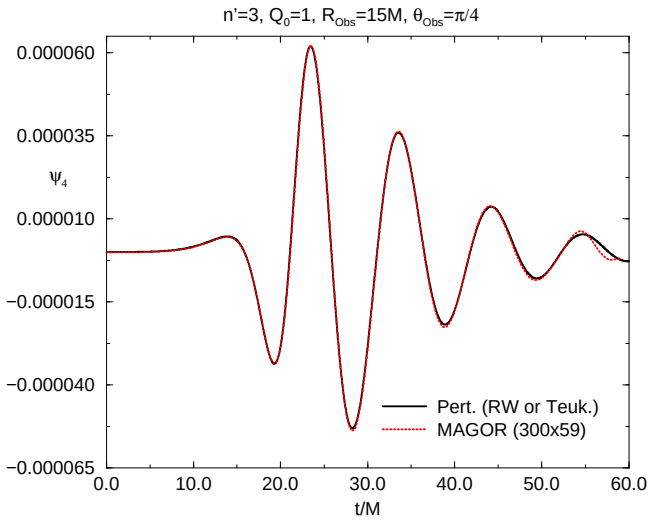


FIG. 8. The Weyl scalar $\psi_4$ as seen by an observer located at isotropic coordinates $\bar{r} = 15M$ and $\theta = \pi/4$. For $n' = 3$ we have a pure $\ell = 3$ linear contribution although no multipole decomposition was made of $\psi_4$. We compare here the results of integrating full (axially symmetric) Einstein equations numerically with the program *Magor* using a resolution of 300 radial and 59 angular zones with the linear evolution of initial data via the Teukolsky equation or the Regge-Wheeler equation and then use the transformation equations (22) to build up $\psi_4$ [only possible in the nonrotating case].

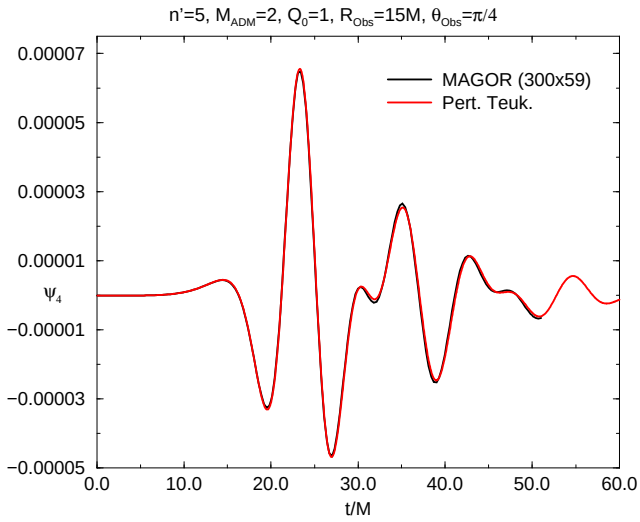


FIG. 9. The Weyl scalar $\psi_4$ for the $n' = 5$ initial data. We observe the beating of the $\ell = 3$ and $\ell = 5$ components since we are not making any multipole decomposition.

with the Teukolsky equation, observed at a constant angular location $\theta = \pi/4$, and the dotted line shows the result of the *Magor* evolution at the same location, with $\psi_4$ extracted from the full nonlinear simulation as described in Sec. II.C.2 above. The results agree extremely well except at very late times, when the nonlinear results are affected slightly by coarse resolution in the outer regions of the numerical grid. We also verify here that the results of the Regge-Wheeler evolution, transformed to provide the same function $\psi_4$ according to Eq. (22) above, agree with the Teukolsky evolution. The results of the two perturbative approaches are indistinguishable in the graph.

We now examine the other family of distorted black holes with the choice of angular parameter $n' = 5$. The initial data were obtained as before, and evolved with the nonlinear *Magor* code and the Teukolsky code. The results are shown in Fig. 9, where we see excellent agreement between the two plots. But notice that the waveform does *not* show the clear quasi-normal mode appearance that one is accustomed to in such plots. This is because this data set has a roughly equal admixture of both $\ell = 3$ and $\ell = 5$ components of radiation, and the curvature based $\psi_4$ approach is not decomposed into separate multipoles. This waveform shows a clear beat of the two $\ell = 3$ and $\ell = 5$ components.

### C. Comparison of nonlinear 2D and full 3D codes

Having successfully tested the 2D fully nonlinear code *Magor* for odd-parity distortions against perturbative evolutions, we can now test the 3D code *Cactus* against the 2D one. In *Cactus*, using the same procedures as in Sec. II C, the initial data are evolved in the full (no octant) 3D mode, with a second order convergence algorithm, maximal slicing, and static boundary conditions. Note we perform the conformal-traceless scheme [42,43] for this evolution. The first observation is that we have to solve the initial value problem taking into account all nonlinearities, even if we are in the linear regime ($Q_0 < 10$), since small violations of the Hamiltonian constraint contaminate the outgoing waveforms.

The runs presented in Figs. 10, 11, and 12 show very nice agreement with the 2D code (hence also with perturbation theory). Note that the spatial resolution ($\Delta x^j = 0.15M = 0.3$) is not high. Here we show waveforms for $t/M \leq 30$. The runs do *not* crash afterwards, but become less accurate due to the low resolution and boundary effects, and even later to collapse of the lapse.

The $\ell-$modes shown in Figs. 10-12 are essentially dominated (for $Q_0 = 2$) by the linear initial distortion of the black hole. Those are the modes that we can compare with first order perturbation theory. Since we have two nonlinear codes we can now compare their predictions for modes dominated by nonlinear effects. That is the case of the odd mode $\ell = 5$ when the initial data parameter is $n' = 3$. This mode has a linear contribution only for $\ell = 3$. For $\ell = 5$ is easy to see that to generate an odd mode we need at least cubic contributions. Thus this mode will scale as $Q_0^3$. To be able to verify the agreement between the 2D and 3D codes we ampli-

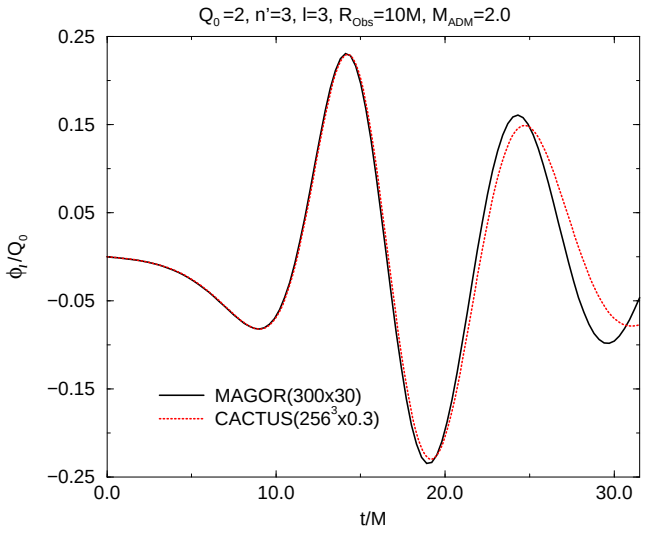


FIG. 10. The $\ell = 3$, odd-parity Moncrief waveform, extracted from the fully nonlinear 3D evolution code *Cactus* (dotted line). The spatial grid consists of $256^3$ points with a separation of $0.15M$. The ADM mass of the black hole is $M = 2.0$ and $(n' = 3, Q_0 = 2, \eta_0 = 2, \sigma = 1)$. For comparison we also plot the results of evolving the same initial data with the fully nonlinear 2D evolution code *Magor* (solid line), which in turn has been tested against perturbation theory as shown in Fig. 3. Very good agreement is reached with a relatively low resolution of the 3D code.

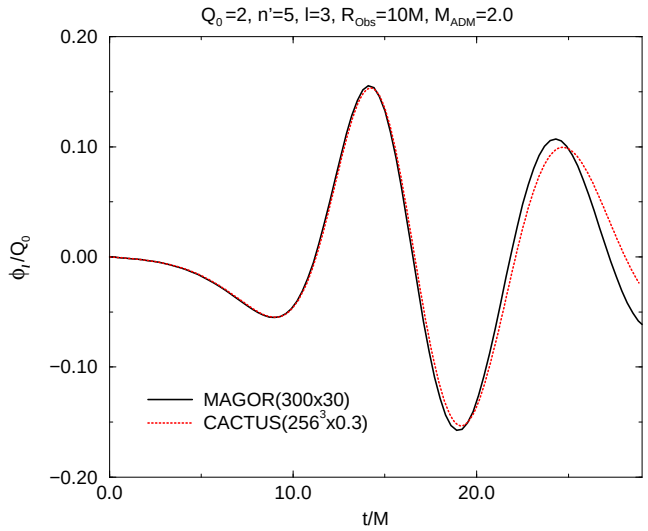


FIG. 11. The $\ell = 3$, odd-parity Moncrief waveform produced by the 3D code *Cactus* (dotted line). It corresponds to initial data with parameters $(n' = 5, Q_0 = 2, \eta_0 = 2, \sigma = 1)$. It also show very good agreement with the 2D results (solid line) which had been checked against perturbation theory as displayed in Fig. 5.

fied this mode taking $Q_0 = 32$ and checked the (almost) quadratic convergence of *Cactus* to the correct results as shown in Fig. 13.

## IV. DISCUSSION

We have completed a series of comparisons covering four different approaches for two classes of odd-parity distortions of Schwarzschild black holes. This includes 2D and 3D nonlinear evolutions and for the first time, in both cases, a comparison of the odd-parity Regge-Wheeler-Moncrief formulation as well as the Teukolsky approach with numerical results. In all cases we find excellent agreement among the different approaches. We emphasize that these matchings have been achieved without the aid of any parameters and thereby stand as a strong verification of these techniques.

Although the distorted black hole initial data configurations we consider here are not necessarily astrophysically relevant, our analysis provides an example of the usefulness of perturbation theory as an interpretive tool for understanding the dynamics produced in fully nonlinear evolutions. In order to distinguish the cases of linear and nonlinear dynamics we simply show the output of the full nonlinear code, but we scale it by the factor $Q_0/M^2$ so that, if the system is responding linearly to $Q_0$ all the waveforms will lie exactly on top of one another. Using this procedure we are able to recognize the emergence of

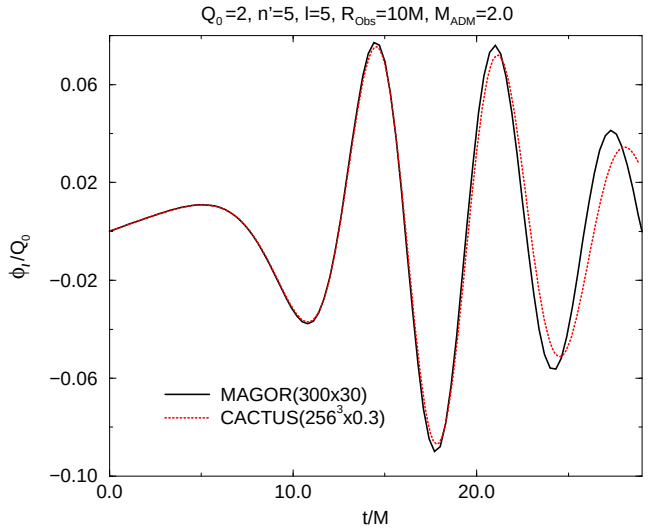


FIG. 12. The $\ell = 5$, odd-parity Moncrief waveform produced by the 3D code *Cactus* (dotted line) with initial data having $(n' = 5, Q_0 = 2, \eta_0 = 2, \sigma = 1)$. Comparison with the 2D results (solid line) show a very good agreement. See Fig. 6 for the agreement between the 2D run and perturbation results.

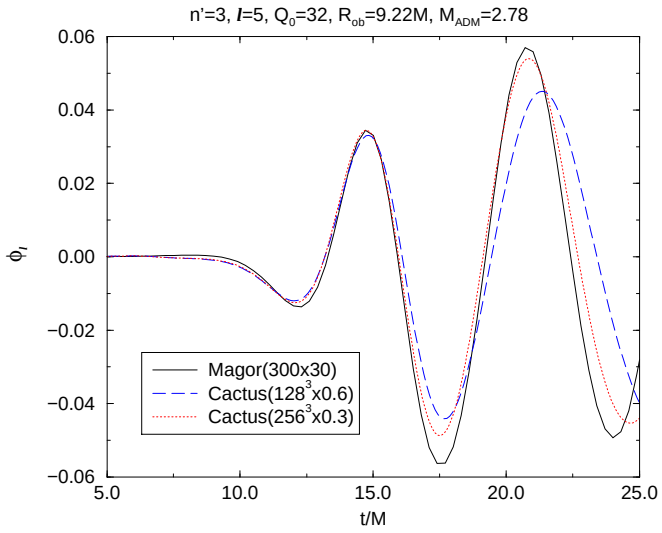


FIG. 13. The $\ell = 5$, odd-parity Moncrief waveform produced by the 3D code *Cactus* (dotted line) with initial data having $(n' = 3, Q_0 = 32, \eta_0 = 2, \sigma = 1)$ and $M_{ADM} = 2.777$. This is a purely nonlinear mode, its leading term being cubic in the amplitude $Q_0$. Comparison with the 2D results (solid line) show a good rate of convergence with the grid spacing (from $\Delta x = 0.6M/2.777$ to $\Delta x = 0.3M/2.777$. See Fig. 7 for the purely 2D runs.

nonlinear dynamics. Considering the mixing of perturbative modes also enables us to understand the results of one case which displays strictly nonlinear behavior, the $\ell = 5$ waveform of the initial data with $n' = 3$ (see Figs. 7 and 13). This wave strictly vanishes to linear order in $\tilde{Q}_0$ and scales at lower amplitudes like $\tilde{Q}_0^3$. The perspective of perturbation theory allows us to create a full picture, identifying and explaining aspects of the nonlinear dynamics even when the perturbations are beyond the linear regime. In this case we find that linearized dynamics provide a very good approximation of the systems' behavior until the radiation constitutes a significant portion of the initial mass, producing a smaller final black hole and, for example, higher quasi-normal ringing frequencies.

Although we restrict to the case where the black hole system does not have net angular momentum, the approach we develop in this paper is completely general, and can easily be extended to the case of distorted black holes with nonvanishing angular momentum. For this reason, we developed a procedure for using the Teukolsky equation to evolve the perturbations on a black hole background, handling both the even- and odd-parity perturbations simultaneously, and providing the capability to deal with perturbations evolving on a Kerr background.

In future work we expect to move in two directions: (a) We will apply the techniques developed here to the case of distorted, rotating black holes, to study nonlinear effects in the radiation of energy and angular momentum as well as to further develop the Teukolsky perturbative evolution paradigm for application to coalescing black hole initial data in a close-limit approximation. (b) We will use these techniques to evolve black hole systems, either from numerically generated initial data, or from partially evolved datasets that have reached a stage where they can be treated via perturbation theory.

## ACKNOWLEDGMENTS

We would like to thank our colleagues at AEI and Penn State, especially Gabrielle Allen. This work was supported by AEI, and by NSF grant PHY-0800973. The nonlinear computations have been performed on a 8 Gbyte SGI Origin 2000 with 32 processors at AEI and a 98 Gbyte Cray T3E with 512 processors at MPI-Garching.

[1] Éanna É. Flanagan and S. A. Hughes, Phys. Rev. D **57**, 4535 (1998), gr-qc/9701039.
[2] Éanna É. Flanagan and S. A. Hughes, Phys. Rev. D **57**, 4566 (1998), gr-qc/9710129.
[3] P. Anninos, D. Hobill, E. Seidel, L. Smarr, and W.-M. Suen, Phys. Rev. D **52**, 2044 (1995).
[4] P. Anninos, K. Camarda, J. Massó, E. Seidel, W.-M. Suen, and J. Towns, Phys. Rev. D **52**, 2059 (1995).
[5] P. Anninos, J. Massó, E. Seidel, and W.-M. Suen, Physics World **9**, 43 (1996).
[6] K. Camarda and E. Seidel, Phys. Rev. D **57**, R3204 (1998), gr-qc/9709075.
[7] R. Gomez, L. Lehner, R. Marsa, J. Winicour, A. M. Abrahams, A. Anderson, P. Anninos, T. W. Baumgarte, N. T. Bishop, S. R. Brandt, J. C. Browne, K. Camarda, M. W. Choptuik, G. B. Cook, R. Correll, C. R. Evans, L. S. Finn, G. C. Fox, T. Haupt, M. F. Huq, L. E. Kidder, S. A. Klasky, P. Laguna, W. Landry, J. Lenaghan, J. Masso, R. A. Matzner, S. Mitra, P. Papadopoulos, M. Parashar, L. Rezzolla, M. E. Rupright, F. Saied, P. E. Saylor, M. A. Scheel, E. Seidel, S. L. Shapiro, D. Shoemaker, L. Smarr, B. Szilagyi, S. A. Teukolsky, M. H. P. M. van Putten, P. Walker, and J. W. Y. Jr, Phys. Rev. Lett. **80**, 3915 (1998), gr-qc/9801069.
[8] S. Brandt and E. Seidel, Phys. Rev. D **54**, 1403 (1996).
[9] S. Brandt and E. Seidel, Phys. Rev. D **52**, 856 (1995).
[10] S. Brandt and E. Seidel, Phys. Rev. D **52**, 870 (1995).
[11] A. Abrahams, D. Bernstein, D. Hobill, E. Seidel, and L. Smarr, Phys. Rev. D **45**, 3544 (1992).
[12] D. Bernstein, D. Hobill, E. Seidel, L. Smarr, and J. Towns, Phys. Rev. D **50**, 5000 (1994).
[13] P. Anninos, D. Hobill, E. Seidel, L. Smarr, and W.-M. Suen, Phys. Rev. Lett. **71**, 2851 (1993).
[14] P. Anninos and S. Brandt, Phys. Rev. Lett. **81**, 508 (1998).
[15] J. Baker, A. Abrahams, P. Anninos, S. Brandt, R. Price, J. Pullin, and E. Seidel, Phys. Rev. D **55**, 829 (1997).

[16] P. Anninos, R. H. Price, J. Pullin, E. Seidel, and W.-M. Suen, Phys. Rev. D **52**, 4462 (1995).
[17] J. Pullin, in *Proceedings of GR15*, edited by N. Dadhich and J. Narlikar (Inter Univ. Centre for Astr. and Astrop., Puna, 1998), p. 87.
[18] G. Allen, K. Camarda, and E. Seidel, (1998), gr-qc/9806014, submitted to Phys. Rev. D.
[19] G. Allen, K. Camarda, and E. Seidel, (1998), gr-qc/9806036, submitted to Phys. Rev. D.
[20] M. Campanelli and C. Lousto, Phys. Rev. D **59**, 124022 (1999), gr-qc/9811019.
[21] A. M. Abrahams, L. Rezzolla, M. E. Rupright, A. Anderson, P. Anninos, T. W. Baumgarte, N. T. Bishop, S. R. Brandt, J. C. Browne, K. Camarda, M. W. Choptuik, G. B. Cook, R. R. Correll, C. R. Evans, L. S. Finn, G. C. Fox, R. Gomez, T. Haupt, M. F. Huq, L. E. Kidder, S. A. Klasky, P. Laguna, W. Landry, L. Lehner, J. Lenaghan, R. L. Marsa, J. Masso, R. A. Matzner, S. Mitra, P. Papadopoulos, M. Parashar, F. Saied, P. E. Saylor, M. A. Scheel, E. Seidel, S. L. Shapiro, D. Shoemaker, L. Smarr, B. Szilagyi, S. A. Teukolsky, M. H. P. M. van Putten, P. Walker, J. Winicour, and J. W. Y. Jr, Physical Review Letters **80**, 1812 (1998), gr-qc/9709082.
[22] A. M. Abrahams, S. L. Shapiro, and S. A. Teukolsky, Phys. Rev. **D51**, 4295 (1995).
[23] M. Campanelli, W. Krivan, and C. Lousto, Phys. Rev. D **58**, 024016 (1998).
[24] A. Lichnerowicz, J. Math Pures et Appl. **23**, 37 (1944).
[25] J. Bowen and J. W. York, Phys. Rev. D **21**, 2047 (1980).
[26] T. Regge and J. Wheeler, Phys. Rev. **108**, 1063 (1957).
[27] F. J. Zerilli, Phys. Rev. D. **2**, 2141 (1970).
[28] V. Moncrief, Annals of Physics **88**, 323 (1974).
[29] S. A. Teukolsky, Astrophys. J. **185**, 635 (1973).
[30] M. Campanelli, C. O. Lousto, J.Baker, G.Khanna, and J. Pullin, Phys. Rev. D **58**, 084019 (1998).
[31] W. Krivan, P. Laguna, P. Papadopoulos, and N. Andersson, Phys. Rev. D **56**, 3395 (1997).
[32] M. Campanelli and C. Lousto, Phys. Rev. D **58**, 024015 (1998).
[33] C. O. Lousto, (1999), preprint AEI-1999-6.
[34] S. Brandt, J. A. Font, J. M. Ibáñez, J. Massó, and E. Seidel, Phys. Rev. D (1998), submitted, gr-qc/9807017.
[35] A. Abrahams and C. Evans, Phys. Rev. D **37**, 318 (1988).
[36] E. Seidel, in *Sixth Marcel Grossman Meeting on General Relativity (Proceedings, Kyoto, Japan, 1991)*, edited by H. Sato and T. Nakamura (World Scientific, Singapore, 1992).
[37] V. Moncrief, Annals of Physics **88**, 343 (1974).
[38] F. J. Zerilli, Phys. Rev. Lett. **24**, 737 (1970).
[39] L. Gunnarsen, H. Shinkai, and K. Maeda, Class. Quantum Grav. **12**, 133 (1995).
[40] M. Shibata and T. Nakamura, Phys. Rev. D **52**, 5428 (1995).
[41] T. W. Baumgarte and S. L. Shapiro, Physical Review D **59**, 024007 (1999).
[42] M. Alcubierre, G. Allen, B. Brügmann, E. Seidel, and W.-M. Suen, (1999), gr-qc/9908079.
[43] M. Alcubierre, G. Allen, B. Brügmann, T. Dramlitsch, J. Font, M. Miller, P. Papadopoulos, E. Seidel, N. Stergioulas, W.-M. Suen, R. Takahashi, and M. Tobias, in preparation (1999).